

# Rotational Raman generation with near-unity conversion efficiency

D. D. Yavuz, D. R. Walker, G. Y. Yin, and S. E. Harris

*Edward L. Ginzton Laboratory, Stanford University, Stanford, California 94305*

Received August 24, 2001

We demonstrate collinear generation of equidistant rotational sidebands in low-pressure molecular hydrogen with near-unity conversion efficiency. The spectrum consists of 37 coherent sidebands covering over 20,000  $\text{cm}^{-1}$  of spectral bandwidth and ranging from 1.37  $\mu\text{m}$  to 352 nm in wavelength. © 2002 Optical Society of America

OCIS codes: 020.1670, 190.5650, 190.7110, 320.2250.

It has been predicted that a highly coherent Raman medium will generate a collinearly propagating comb of sidebands with many octaves of spectral bandwidth. This is achieved by driving a Raman resonance with two single-mode laser fields whose frequency difference is slightly detuned from the Raman resonance and whose intensity is sufficiently large to cause the magnitude of the coherence of this transition to be of the order of its maximum value,  $|\rho_{ab}| \approx 0.5$ . When this is the case, the generation and phase-slip lengths become comparable and Raman generation proceeds collinearly, with off-axis phase matching playing a negligible role. Molecular motion, either in phase (below-resonance excitation) or out of phase (above-resonance excitation) with the driving force, modulates the driving laser frequencies, causing the generation of a very broad FM-like spectrum.<sup>1</sup> In earlier experiments in our group, we used lasers at 1.06  $\mu\text{m}$  and 807.2 nm to drive the fundamental vibrational transition in molecular deuterium ( $\text{D}_2$ ) at 2994  $\text{cm}^{-1}$ . Seventeen mutually coherent sidebands with wavelengths from 2.94  $\mu\text{m}$  to 195 nm were observed.<sup>2</sup> These sidebands had sufficient power to allow the observation of phase-controlled, multiphoton ionization of Xe and the inference of single-cycle pulses with pulse lengths of  $\sim 2$  fs.<sup>3</sup> In closely related work, Hakuta and co-workers reported the generation of a comb of vibrational sidebands in solid hydrogen<sup>4</sup> ( $\text{H}_2$ ) and rovibrational sidebands in a liquid- $\text{H}_2$  droplet.<sup>5</sup>

In this Letter we extend the off-resonant Raman generation technique to rotational transitions.<sup>6</sup> By using the  $\nu'' = 0, J'' = 1 \rightarrow \nu' = 0, J' = 3$  transition in molecular  $\text{H}_2$ , we demonstrate collinear generation of a rotational Raman spectrum extending over 20,000  $\text{cm}^{-1}$ . The observed spectrum consists of 37 coherent sidebands spaced by 587  $\text{cm}^{-1}$ , with wavelengths from 1.37  $\mu\text{m}$  to 352 nm. Allowing for temporal overlap factors, the conversion efficiency from the two driving lasers to the generated spectrum is nearly unity. To our knowledge, this is the first observation of a broad rotational Raman spectrum in the low-pressure, high-coherence regime and the first investigation of off-resonant rotational excitation. The mutually coherent narrow-linewidth sidebands produced may be used to synthesize femtosecond-time-scale pulses. A special feature of

Ti:sapphire-driven rotational systems is that, by simultaneously tuning the frequency of both driving lasers while keeping the difference of their frequencies constant, one may generate sidebands that tune continuously from the mid infrared to the far ultraviolet.

Before proceeding further, we note connections to other earlier and pertinent work: (1) Imasaka and co-workers<sup>7,8</sup> and Losev and co-workers<sup>9,10</sup> suggested two-color excitation of a Raman resonance and demonstrated generation of a broad rotational spectrum in the low-coherence, high-pressure regime. They observed a small divergence of the anti-Stokes beams and increased conversion efficiency compared with traditional stimulated Raman scattering. (2) Recently, Nazarkin and colleagues demonstrated efficient Raman generation by impulsive excitation of coherent vibrations in  $\text{SF}_6$  and coherent rotations in  $\text{H}_2$ .<sup>11,12</sup> (3) The technique that we use here, adiabatic excitation of maximum coherence, is closely related to the work of Jain *et al.*<sup>13</sup> and Merriam *et al.*,<sup>14</sup> who demonstrated near-unity conversion efficiency in Pb vapor.

The experimental setup of this work is shown in Fig. 1. The rotational resonance is driven by two tunable laboratory-built Ti:sapphire laser systems at wavelengths of 797 and 836 nm. Each laser is injection seeded from an external-cavity laser diode and pumped by the second harmonic of a Q-switched Nd:YAG laser (Quanta-Ray). These lasers produce

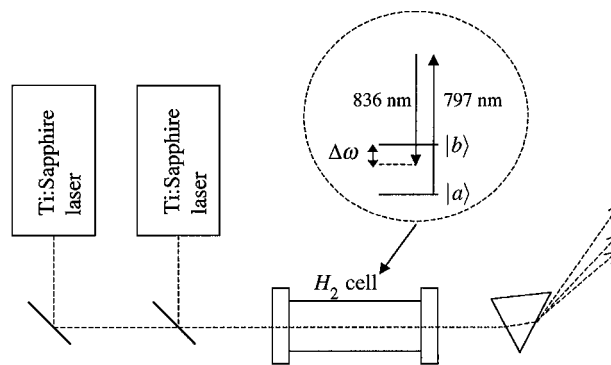


Fig. 1. Experimental setup and energy-level diagram for collinear rotational Raman generation. With  $\Delta\omega$  as shown, the phased rotational eigenstate is excited.

60-mJ transform-limited pulses at the seeding laser wavelength, with pulse durations of 17 and 14 ns, respectively. The seeding wavelengths can be tuned and are monitored by a Burleigh WA-1500 wavemeter with a resolution of 50 MHz. The frequency difference between these two lasers is tuned to cause above-resonance, below-resonance, or on-resonance excitation of the rotational transition. The laser pulses are synchronized and combined on a dichroic beam splitter and are focused to a spot size of  $\sim 400 \mu\text{m}$ . The intensity of each of the lasers at the midcell focal point is  $\sim 2 \text{ GW}/\text{cm}^2$ .

The  $\text{H}_2$  cell is 50 cm long and is cooled by liquid nitrogen ( $\text{N}_2$ ) to a temperature of 77 K. Cooling reduces the Doppler linewidth to 72 MHz and increases the population of the  $J'' = 1$  rotational state to 75%. The pressure of the  $\text{H}_2$  cell is set at 250 Torr. We determine the Raman resonance by two methods. In the first method we measure weak 836-nm laser gain while scanning its frequency with the 797-nm laser frequency fixed. The gain is expected to peak at the pressure-shifted resonance. In the second method we put a commercial audio microphone in the  $\text{H}_2$  cell and measure the amplitude of the shock wave produced by laser energy that is absorbed in the medium. Since the absorption is due to nonadiabatic behavior, the amplitude of the shock wave also peaks on resonance. Within our spectral resolution, these two measurements give the same value for the  $\nu'' = 0, J'' = 1 \rightarrow \nu' = 0, J' = 3$  rotational transition. This value is  $587.03 \text{ cm}^{-1}$ .

When we apply full power to our driving lasers and tune the frequency difference of the two lasers close to Raman resonance, we see a bright beam of white light at the output of the cell. We observe generation of as many as 27 anti-Stokes and 8 Stokes sidebands in addition to the two driving lasers. The spectrum is dispersed with a prism and projected on white paper. Figure 2 shows a photograph of the generated spectrum for three different Raman detuning values  $\Delta\omega$ . The near-Gaussian transverse profiles in this photograph demonstrate the collinear nature of the spectrum. The high-order anti-Stokes generation is more efficient for below-resonance excitation (phased molecular state) than for above-resonance (antiphased state) and on-resonance excitation. This difference was also observed for vibrational excitation in  $\text{D}_2$  (Ref. 2) and may be due to Raman self-focusing.<sup>15</sup> Figure 3 shows the energies for the 17 central sidebands for the spectrum of Fig. 2(c).

Figure 4 shows the total generated energies in the Stokes and anti-Stokes sidebands as a function of Raman detuning. We find that the Stokes sideband generation peaks, whereas anti-Stokes generation shows a slight dip for on-resonance excitation. Qualitatively, this behavior can be explained in the following way: For on-resonance excitation, the energy flows from the driving lasers to the molecules and is left in the molecules as a result of nonadiabatic behavior. During this energy flow, 797-nm photons are absorbed and 836-nm photons are amplified. As a result, the Stokes generation peaks and the anti-Stokes generation shows a slight dip. For off-resonant excitation, the energy flows adiabatically, first from the fields to

the molecules, then from the molecules to the fields, and therefore this effect is not present.

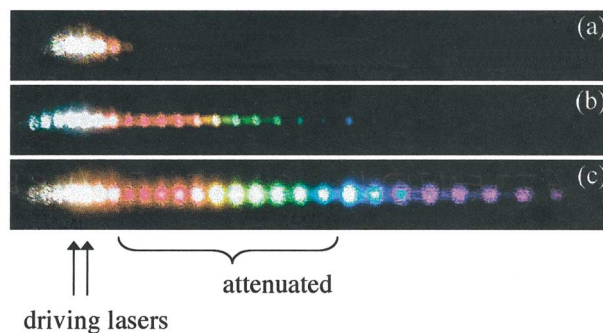


Fig. 2. Generated rotational spectrum at Raman detuning values of (a)  $\Delta\omega = -80 \text{ MHz}$ , (b)  $\Delta\omega = 0$ , (c)  $\Delta\omega = 280 \text{ MHz}$ . The middle portion is attenuated to reduce camera saturation. For below-resonance excitation, we observe generation of 27 anti-Stokes and 8 Stokes sidebands (in addition to the driving lasers).

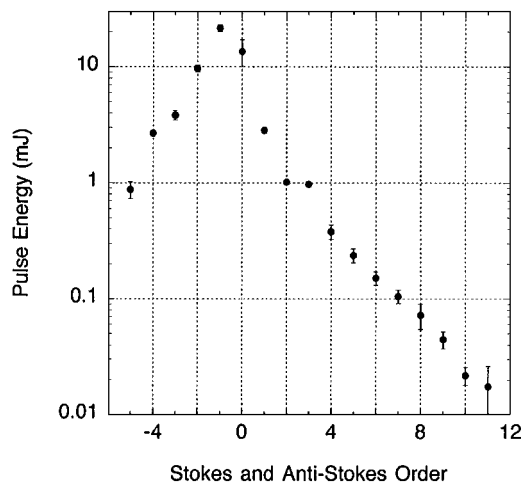


Fig. 3. Integrated pulse energies for the observed spectrum of Fig. 2(c). The sideband numbered 0 is the 797-nm driving laser.

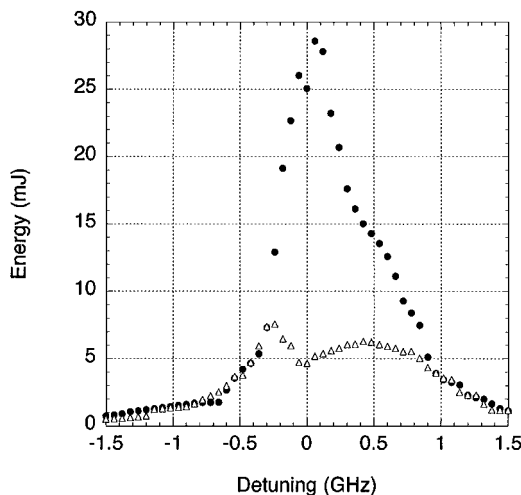


Fig. 4. Total generated Stokes (circles) and anti-Stokes (triangles) energy as a function of Raman detuning. The Stokes generation peaks, and the anti-Stokes generation shows a slight dip for on-resonance excitation.

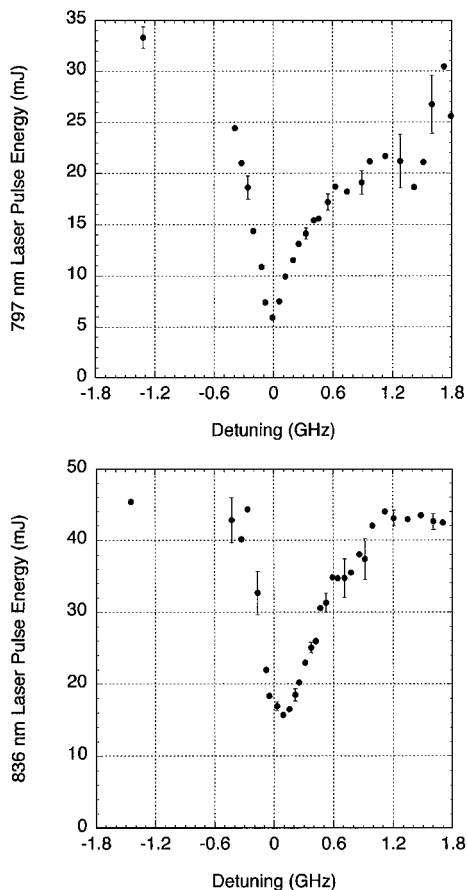


Fig. 5. Depletion of two driving lasers as a function of Raman detuning. At the peak of the generation, the depletion of both lasers is  $\sim 70\%$ . Accounting for overlap factors, these values approach 100%, implying near-unity conversion from the driving lasers to the generated spectrum.

Figure 5 shows the depletion of the two driving lasers as a function of two-photon detuning. The observed depletion of both lasers is  $\sim 70\%$  without considering overlap factors. Accounting for overlap factors, these values approach 100%, implying near-unity conversion from the driving lasers to the generated spectrum. This high efficiency is a result of operating near maximum molecular coherence (the highest molecular coherence that is achieved in our experiment is calculated to be  $|\rho_{ab}| \approx 0.3$ ). All measurements for Figs. 4 and 5 were done with a Molecron J4-09 pyroelectric detector.

In conclusion, we have demonstrated collinear generation of a wide rotational Raman spectrum in low-density molecular  $H_2$  with, allowing for temporal overlap factors, near-unity conversion efficiency. As noted above, because both driving lasers may be simultaneously tuned, this source may produce continuously tunable radiation over much of the visible, UV, and IR spectra. Pumping with frequency-doubled Ti:sapphire lasers would produce an attractive

source with continuous tunability in the 250–500-nm range. Other applications include (1) the synthesis of femtosecond-time-scale pulses with repetition periods that are longer (in this case 56.7 fs) than are obtainable with vibrational transitions, (2) the synthesis of electromagnetically induced transparency-like<sup>16</sup> and self-induced transparency-like<sup>17</sup> solitons, and (3) application to the recently suggested multiplicative Raman technique. This last technique allows a total number of sidebands that is equal to the product of the number of sidebands of two independent Raman cells and, at the same time, pulses that are produced at random times with average temporal spacings of picoseconds.<sup>18</sup>

D. D. Yavuz and D. R. Walker contributed equally to this work. The authors thank Alexei Sokolov for helpful discussions and for his assistance with the experiment. This work was supported by the U.S. Air Force Office of Scientific Research, the U.S. Army Research Office, and the U.S. Office of Naval Research. D. R. Walker acknowledges support from the Fannie and John Hertz Foundation. S. E. Harris's e-mail address is seharris@ee.stanford.edu.

## References

1. S. E. Harris and A. V. Sokolov, *Phys. Rev. Lett.* **81**, 2894 (1998).
2. A. V. Sokolov, D. R. Walker, D. D. Yavuz, G. Y. Yin, and S. E. Harris, *Phys. Rev. Lett.* **85**, 562 (2000).
3. A. V. Sokolov, D. R. Walker, D. D. Yavuz, G. Y. Yin, and S. E. Harris, *Phys. Rev. Lett.* **87**, 033402 (2001).
4. J. Q. Liang, M. Katsuragawa, F. Le Kien, and K. Hakuta, *Phys. Rev. Lett.* **85**, 2474 (2000).
5. S. Uetake, M. Katsuragawa, M. Suzuki, and K. Hakuta, *Phys. Rev. A* **61**, 011803 (1999).
6. A. V. Sokolov, D. D. Yavuz, and S. E. Harris, *Opt. Lett.* **24**, 557 (1999).
7. T. Imasaka, S. Kawasaki, and N. Ishibashi, *Appl. Phys. B* **49**, 389 (1989).
8. H. Kawano, Y. Hirakawa, and T. Imasaka, *IEEE J. Quantum Electron.* **34**, 260 (1998).
9. L. L. Losev and A. P. Lutsenko, *Quantum Electron.* **23**, 919 (1993).
10. G. S. McDonald, G. H. C. New, L. L. Losev, A. P. Lutsenko, and M. Shaw, *Opt. Lett.* **19**, 1400 (1994).
11. A. Nazarkin, G. Korn, M. Wittman, and T. Elsaesser, *Phys. Rev. Lett.* **83**, 2560 (1999).
12. M. Wittman, A. Nazarkin, and G. Korn, *Opt. Lett.* **26**, 298 (2001).
13. M. Jain, H. Xia, G. Y. Yin, A. J. Merriam, and S. E. Harris, *Phys. Rev. Lett.* **77**, 4326 (1996).
14. A. J. Merriam, S. J. Sharpe, H. Xia, D. Manuszak, G. Y. Yin, and S. E. Harris, *Opt. Lett.* **24**, 625 (1999).
15. S. E. Harris and A. V. Sokolov, *Phys. Rev. A* **55**, R4019 (1997).
16. D. D. Yavuz, A. V. Sokolov, and S. E. Harris, *Phys. Rev. Lett.* **84**, 75 (2000).
17. A. E. Kaplan, *Phys. Rev. Lett.* **73**, 1243 (1994).
18. S. E. Harris, D. R. Walker, and D. D. Yavuz, *Phys. Rev. A* **65**, 021801 (2002).